

PACS numbers: 43.35.+d, 81.05.uj, 81.40.Rs, 82.47.Uv, 84.32.Tt, 88.85.jp, 89.20.Bb

Size Effects at Ultrasonic Treatment of Nanoporous Carbon and Improved Characteristics of Supercapacitors on Its Base

O. V. Balaban, B. Ya. Venhryn, I. I. Grygorchak, S. I. Mudry*,
Yu. O. Kulyk*, B. I. Rachiy**, and R. P. Lisovskiy**

*Lviv Polytechnic National University,
12 Bandera Str.,
79013 Lviv, Ukraine*

**Ivan Franko National University of Lviv,
8 Kyrylo and Mefodij Str.,
79005 Lviv, Ukraine*

***Vasyl Stefanyk Pre-Carpathian National University,
57 Shevchenko Str.,
76018 Ivano-Frankivsk, Ukraine*

As shown, the common characteristic for nanoporous carbons obtained from different types of natural raw materials is so called fractal geometry, which changing is substantially reflected on the process of capacitive energy storage in an electric double layer (EDL) formed at the boundary between the carbon material and the electrolyte (KOH 30% aqueous solution). Relationship between the parameters of fractality and features of ultrasonic influence of carbon on the electronic structure and the structure of the EDL is investigated and results in establishing conditions to achieve improved performance characteristics of supercapacitors based on them.

В роботі вперше знайдено спільну характеристику для нанопористих вуглеців, одержаних із різних видів природної сировини, — фрактальну геометрію, зміна якої істотно відбивається на процесі місткісного накопичення енергії в подвійному електричному шарі (ПЕШ) на роздільчій межі вуглецевого матеріалу з 30% водним розчином КОН. З'ясовано взаємозв'язок між параметрами фрактальності та впливом ультразвукового опромінення на електронну будову і структуру ПЕШ, встановлено умови для поліпшення експлуатаційних характеристик суперконденсаторів.

В работе впервые обнаружена общая характеристика нанопористых углеродов, полученных из различных видов природного сырья, — фрактальная геометрия, изменение которой существенно отражается на процессе ёмкостного накопления энергии в двойном электрическом слое (ДЭС) на границе раздела углеродного материала с 30% водным раствором КОН.

Установлена взаимосвязь между параметрами фрактальности и влиянием ультразвукового облучения на электронное строение и структуру ДЭС, определены условия для улучшения эксплуатационных характеристик суперконденсаторов.

Key words: ultrasound, carbon, capacitance, fractality, electric double layer.

(Received 7 April, 2014)

1. INTRODUCTION

Significant efforts in the field of high-power efficient accumulation and energy storage systems have led to an increase of operating voltage of single elements for lithium-ion batteries up to 4.5–4.7 V [1, 2]. However, this progress is insufficient, because the power density of such elements remains low. It is believed that to overcome this problem an optimal combination of porous structure and appropriate electron structure of the material should be used. Helmholtz capacitance unblocking by the spatial charge region (SCR) capacitance in the solid phase can be successful for this purpose.

Combination described above can be implemented using supercapacitors with capacitive or pseudocapacitive energy storage mechanisms. Known chemical methods for modification of porous structure [3–7] previously used for this purpose do not provide the required electron structure change. Now, it is clear that in order to overcome this problem, it is necessary to find a characteristic of activated carbon, which changing would lead to the desired and controlled conjugate modification of porous structure and electron structure, and to find a way of such influence.

At the same time, taking into account the stringent market requirements connected with cost of one-Farad capacitance and environmental safety inevitably generates the necessity to use elimination of harmful substances as the initial materials for activated carbonization and precursors for further modification.

This work is devoted to one of the first steps to solve this threefold task. It is offering a completely new method for this purpose, namely, the ultrasonic treatment (UST).

However, today, the predominant array of papers about improving the active material of supercapacitors is unreasonably associated with modification of their pore structure only [8–11]. Besides, this array is associated with the access to the surface of certain functional redox groups [12–14] without proper attention to providing the required electronic structure and minimizing harmful effects on the environment.

2. BACKGROUND

Ability to combine an optimum porous structure and an appropriate electron structure of the material depends on the peculiarities of the EDL structure formed between the electrolyte and non-metallic solid phase (Fig. 1, *a*) and generalized characteristics of nanoporous carbon. Structure of the EDL certainly implies the existence of SCR capacitance in the solid phase, C_{SC} , in the simplest equivalent electric circuit (Fig. 1, *b*). This capacitance obviously can block the Helmholtz capacitance. According to the scheme in Fig. 1, *b*, the total capacity of the EDL is determined by the relation:

$$C^{-1} = C_{SC}^{-1} + C_H^{-1} + C_G^{-1}, \quad (1)$$

where C_H is the Helmholtz capacitance, C_G is the Gouy–Chapman capacitance of the diffusive layer in the electrolyte and usually is significantly higher than the capacity of the dense EDL that is the Helmholtz layer. The problem of blocking is virtually absent in metal electrodes. However, it is relevant for carbon-graphite electrodes, because Debye screening radius can be quite significant in the last one. It is clear that increasing of C_{SC} promotes the unblocking of the Helmholtz capacitance; C_{SC} is proportional to the density of states at the Fermi level $D(E_F)$ according to the known relation [15]:

$$C_{SC} = e_0 \sqrt{\varepsilon_{SC} \varepsilon_0 D(E_F)}, \quad (2)$$

where ε_{SC} is the relative dielectric constant of the SCR, ε_0 is the vacuum dielectric constant, e_0 is the electron charge.

Actually, modification technology should provide the increasing of C_{SC} . However, it is not only and not obvious condition. Really, C_{SC} capacitance can be blocked by parallel conductivity, which is determined

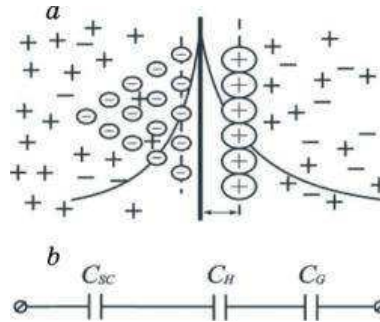


Fig. 1. Model of the EDL for non-metallic electrodes (*a*) and related electric circuit (*b*).

not only by concentration of delocalized carriers (which is proportional to the $D(E_F)$), but also by their mobility, which in nanoporous carbon composites is percolation and therefore it depends on fractal geometry [16–18]. That is why the last can be the one ‘target’ for modification that will promote solution of the problem. We offer to use the ultrasonic irradiation, the action of which should lead to changes in fractality [19] and the consequent modification of the EDL structure parameters and to direct ultrasonic influence on the impurity subsystem [20].

3. EXPERIMENT

In the experiments, nanoporous carbons are used and obtained by the activation carbonization of birch charcoal (BCC), fruit seeds (FSC) and flax fibres (FFC). Ultrasonic treatment with frequency of 22 kHz is performed in the liquid medium using a piezoceramic dispersant. KOH 30% aqueous solution is chosen as an electrolyte.

The method of small-angle X-ray scattering (SAXS) is used to study the fractal structure of the material. The experiments are carried out using a DRON-3 diffractometer. Ge single crystal is installed in the incident beam in order to obtain the CuK_α radiation with a wavelength of 1.5418 Å. In order to reduce the parasite scattering from the crystalline monochromator, a special slit system is arranged ahead the sample. This system can be shifted to ± 4 mm in the direction perpendicular to the X-ray beam. The usage of a perfect Ge crystal and the collimation system described above enabled us to carry out investigations starting from wave vector of $s = 0.01 \text{ \AA}^{-1}$. The slit width of 0.1 mm, which corresponds to the spatial separation $\Delta(2\theta) = 0.03^\circ$ is installed before the detector. The scattered intensities are measured in the transmission regime with a step of $\Delta(2\theta) = 0.05$ degrees within the $0.25\text{--}4.0^\circ$ range and the exposition of 100 s. In order to obtain diffraction curves in a wide angular range, the slit width of 1.00 mm is set before the detector. The low-temperature nitrogen adsorption–desorption method using porometer ‘Quntachrome 4200e’ and software ‘NOVA Win-2.1’ is carried out for porous structure to compare SAXS-data.

The electrochemical studies of activated carbon are performed in a triode cell with a chlorine–silver reference electrode. The impedance measurements are carried out over the frequency range of $10^{-3}\text{--}10^6$ Hz by means of the AUTOLAB (ECO CHEMIE, the Netherlands) measuring set, driven by FRA-2 and GPES software. Creating of impedance models is carried out by the ZView 2.3 (Scribner Associates) software package. The cyclic voltammograms for electrochemical cells are recorded with a sweep voltage rate of 0.01 V/s. The charge–discharge galvanostatic cycles are performed by means of an electronic galvanostatic device.

Micro-Raman measurements are carried out in the backscattering geometry at room temperature using above-mentioned spectrometer and thermoelectrically cooled charge-coupled device (CCD) detector. Ar⁺/Kr⁺ laser (488.0 nm) is used as excitation source. The laser power is changed in the range of 0.25–25 mW. The samples are placed on a computer-controlled XY table with a displacement step of 0.1 μm . The Olympus BX41 confocal optical microscope equipped with a $\times 100$ (numerical aperture is equal to 0.90) is used to focalize the laser light on the sample and collect the scattered light to the spectrometer. A 100 μm confocal diameter diaphragm is placed at the back focal plane of the objective provided the lateral submicron resolution of the measurements. The specific surface area of materials is calculated by density functional theory (DFT) and Barrett–Joyner–Halend (BJH) methods.

4. RESULTS AND DISCUSSION

After sift of BCC through the sieve, the following dimension fraction particles before and after ultrasonic irradiation of initial nanoporous synthesized BCC are allocated: less than 40, 40–63, 63–80, 80–90, 90–200, and more than 200 μm (Table 1). The strongest crushing effect of ultrasonic influence occurs for fraction of the highest dimension within 90–200 μm .

Figure 2 shows the results of measuring of the galvanostatic charge-discharge cycles of the boundary with potassium hydroxide 30% aqueous solution of each BCC fraction before and after ultrasonic irradiation. One can see that before ultrasonic influence the specific capacity is almost (within experimental error) unchangeable, but after influence it changes non-monotonically depending on the particle size of activated BCC. To understand the nature of the observed dependence, fractal analysis is performed of fractions for which the most essential decrease (40–63 μm fraction) and increase (80–90 μm fraction) of specific capacity are identified.

TABLE 1. Content of each dimensional fraction of BCC before and after the ultrasonic treatment.

Fractions, μm	Percent of the total weight	
	Before UST	After UST
< 40	2.87	17.18
40–63	17.88	43.35
63–80	5.16	21.80
80–90	0.87	4.74
90–200	72.18	12.14
> 200	1.04	0.79

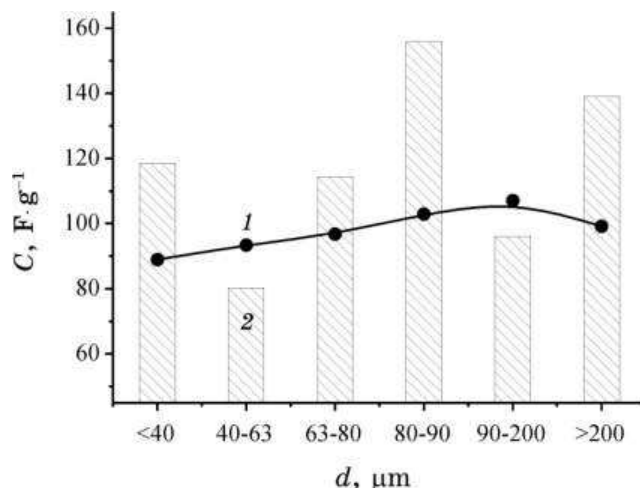


Fig. 2. The specific capacity of the interface of BCC and KOH 30% aqueous solution for investigated fractions before (1) and after (2) the ultrasonic treatment.

Figure 3 shows a typical curve for the intensity of SAXS of investigated fractions before and after the ultrasonic treatment. One can see in a wide range of the wave vector values [s_0, s_{max}] ($s_{\text{max}} = 0.327 \text{ \AA}^{-1}$ is upper experiment limit) there is clearly expressed area with a linear dependence of $\lg I(s)$ vs. $\lg s$, the slope of which ($3 < n < 4$) indicates the scattering of the two-phase porous system and the interface phase which shows fractal behaviour. The surface fractal dimension of the initial materials $D_s = 6 - n = 2.50$ is independent from the average par-

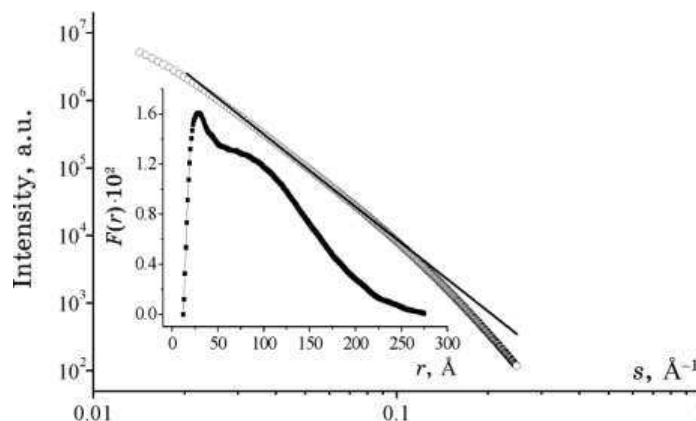


Fig. 3. The dependence of the X-rays scattering intensity on wave vector. Inset is a function of pore volume distribution versus their size.

tics fraction size and decreases to values of $D_s = 2.45$ (40–63 μm) and $D_s = 2.40$ (80–90 μm) after ultrasonic treatment. A deviation from the linear dependence on the intensity curves is due mainly to two reasons:

a) in the region of small scattering angles, the deviation is connected with the transition of scattering mechanism to the Guinier regime [21];

b) for larger scattering angles, the deviation caused by the scattering of individual micropores surface as a part of fractal aggregates.

Functions of the pore volume distribution almost revealed no change after the ultrasonic treatment. It may be noted only insignificant ($\cong 4\%$) increase of the average radius of the pores in the 40–63 μm BCC fraction after the ultrasonic treatment. Calculated according to these data, the active surface area [22] after ultrasonic influence for 40–63 μm fraction decreased for $\cong 1.2\%$, and increased for $\cong 2.8\%$ for 80–90 μm fraction. This only coincides with the change direction and specific capacity change for appropriate fractions, but obviously cannot be its explanation.

Nanoporous carbon obtained from fruit seeds has the fractal structure of surface. Its fractal dimension is higher than the same parameter of BCC and constitutes 2.75. After ultrasonic influence, it is reduced analogously to BCC (80–90 μm fraction) and causes increase of specific capacity, however, by smaller percentage of 15%. However, as opposed to the BCC, the pore-size distribution function radically changes in this case (Fig. 4). In both cases, pore sizes are distributed within the range of 0–42 nm. However, a pronounced isolated maximum, which corresponds to micropores of the most probable size of $d_p = 1.9$ nm in the UST sample is observed on the curve $F(d)$. At the same time, the most probable pore size in the initial sample is equal to $d_p = 4.6$ nm. Figure 5 shows the histograms of the specific capacitance of FSC for various durations of ultrasonic influence and, for comparison, the pore distribution function versus their diameters obtained by the nitrogen sorption–desorption method. Comparing the SAXS data with low-temperature porometry results, we can conclude that the value of the most probable pore diameter in the ultrasonic modified material coincides with the porometry data processed using DFT [23] method, and the original material with the same accuracy with the porometry data processed using BJH [24] method. The values of the active surface area determined by methods of SAXS and porometry differ no more than for 14% (Table 2).

Comparison of these data with histograms and distribution functions (Fig. 5) indicates that for this type of nanoporous carbon inherent discrepancy in nature and magnitude of the active surface area results in the corresponding changes in specific capacity of appropriate materials.

Unlike the previous two materials, the formation of fractal in vol-

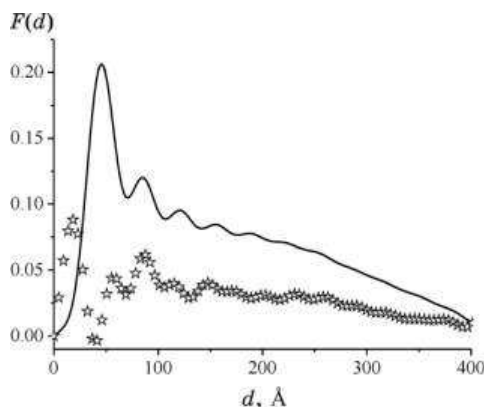


Fig. 4. The pore volume distribution function for FSC versus their size before (solid line) and after (asterisks) the ultrasonic irradiation.

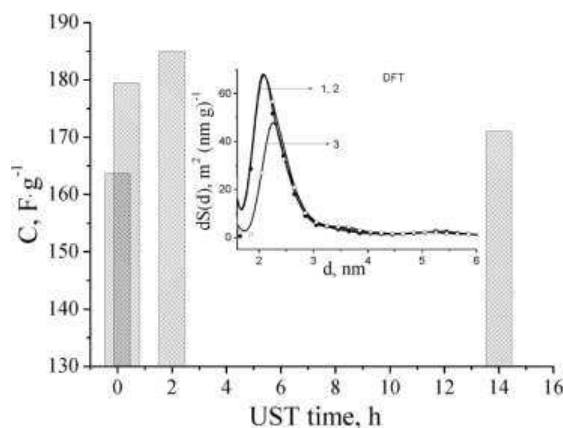


Fig. 5. The specific capacity of the interface of FSC and KOH 30% aqueous solution for different duration of the ultrasonic irradiation. The insert is a pore distribution function versus their diameter after 0.33-hour (1), 2-hour (2) and 14-hour (3) ultrasonic irradiation duration.

ume of structure is observed in the firstly synthesized nanoporous carbon from flax fibres as it is indicated by the value of the slope ($n = 2.75$ ($1 < n < 3$)).

Fractal dimension is estimated to be equal to $D_v = n = 2.75$. One can assume that such structure is formed as a result of aggregation of carbon clusters with diameter, which is close to $d \approx 2L_c$ (L_c is the correlation radius that can be considered as the lower limit of self-similarity of fractal aggregates). For it, the maximum of the distribution function of pores size is in the vicinity of 3.8 nm, and the active surface area is estimated to be $1476 \text{ m}^2 \cdot \text{g}^{-1}$ that is higher than that in the previous

TABLE 2. Change of specific surface area of FSC after the ultrasonic irradiation, calculated by different methods.

Materials Methods	$S, \text{m}^2/\text{g}$			
	Initial	20-min UST	2-h UST	14-h UST
SAXS	1296	1384	—	—
BET	1475	1570	1529	1398
DFT	1426	1502	1475	1350

carbon materials. However, the specific capacitance is of the same order with the BCC one ($100 \text{ F}\cdot\text{g}^{-1}$) and significantly lower (more than 60%) than specific capacitance of FSC. Ultrasonic treatment of FFC results in three times lower increase of specific capacity at the same meaning of the specific capacity of initial BCC.

All these facts indicate that the equivalent electric circuit of the interface of investigated materials and KOH aqueous solution cannot be interpreted by the de Levie classical scheme [25]. It simulates the impedance hodographs that are of the same type for all our tested carbons (Fig. 6), but must contain, according to the Voigt approach, the $R_{sc}C_{sc}$ parallel link, consistently attached (insert to Fig. 6). This link will display the processes that take place in the SCR of solid phase and on which characteristics the ultrasonic irradiation will make effect. Hypothetically, the nature of this effect primarily may be caused by the changes in the relaxation time $\tau_{sc} = (R_{sc}C_{sc})^{-1}$ due to changes in density of states at the Fermi level and/or change of percolation mobility. This mobility will depend on the fractal geometry of the particles of investigated nanoporous materials.

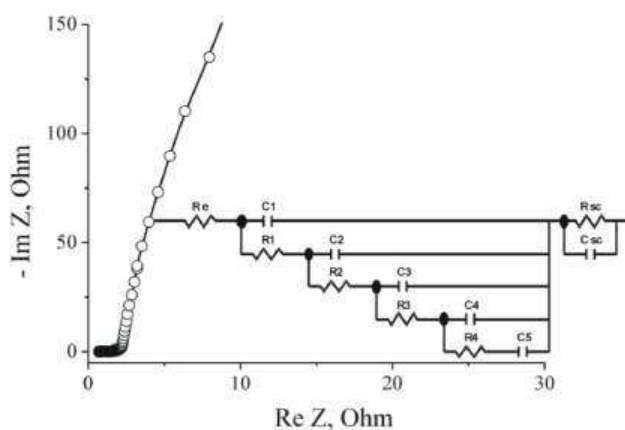

Fig. 6. Nyquist typical diagram for BCC, FSC and FFC. The insert is an equivalent electric circuit.

TABLE 3. Normalized impedance parameters of the model (insert on Fig. 5). Voltage of displacement is equal to $U = 0$ V.

Nanoporous material		$\sum_i R_i, \text{ Ohm/g}$	$\sum_i C_i, \text{ F/g}$	$C_{SC}, \text{ F/g}$	$R_{SC}, \text{ Ohm/g}$
BCC (40–63 μm)	before UST	105.2	0.091	0.033	0.287
	after UST	169.1	0.073	0.047	0.417
BCC (80–90 μm)	before UST	146.9	0.061	0.036	0.558
	after UST	281.6	0.088	0.059	0.388
FSC (80–90 μm)	before UST	167.6	0.056	0.002	0.243
	after UST	104.3	0.028	$8.4 \cdot 10^{-4}$	0.269
FFC (80–90 μm)	before UST	366.9	0.085	$1.2 \cdot 10^{-5}$	0.084
	after UST	2046.7	0.056	0.029	14.101

Results of computer parametric identification of scheme are listed in Table 3.

Value of differential capacitance C_{SC} of SCR and its shunt R_{SC} resistance have changed after ultrasonic irradiation (Table 3). This may be caused by changes in both the density of states at the Fermi level and its position. The fact that the first assumption is realized can be seen from the values of C_{SC} (Table 3). According to (2), change of C_{SC} is adequate to the change of the density of states at the Fermi level. For justification of the second assumption, let us analyse volt–farad dependence of SCR capacitance (Fig. 7, Fig. 8).

Figures 7 and 8 show that the minimums of the C – U dependences are shifting after ultrasonic irradiation. Then, according to [15, 26]:

$$\tilde{\mu}_{E_1} = F_1 - e\phi_{S_1}, \quad \tilde{\mu}_{E_2} = F_2 - e\phi_{S_2}, \quad (3)$$

where e is the electron charge, $\tilde{\mu}_{E_1}$ and $\tilde{\mu}_{E_2}$ are the chemical potentials of each material in the electrolyte, F_1 and F_2 are an appropriate positions of the Fermi level and ϕ_{S_1} and ϕ_{S_2} are the values of potentials, which correspond to minimums on the capacitance-voltage dependences. Since the electrolyte remains intact, then, $\tilde{\mu}_{E_1} = \tilde{\mu}_{E_2}$ and $F_1 - e\phi_{S_1} = F_2 - e\phi_{S_2}$. One can find a shift of the Fermi level after ultrasonic treatment:

$$F_1 - F_2 = e(\phi_{S_1} - \phi_{S_2}). \quad (4)$$

The results of calculation are consolidated in Table 4.

It is important to note that the ultrasonic irradiation causes changes of R_{SC} , which are inconsistent to nature of C_{SC} changes, which are not

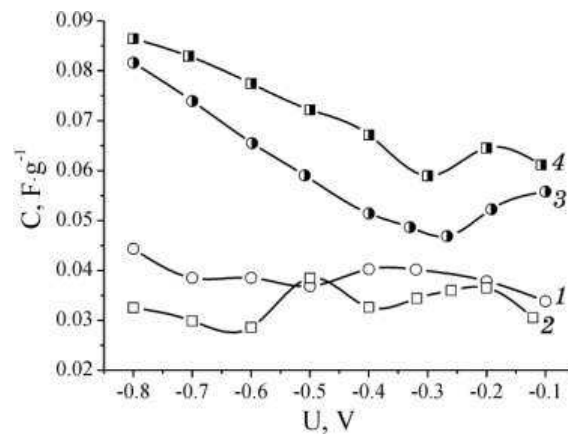


Fig. 7. Volt–farad dependences of SCR for BCC fractions of 40–63 μm (1, 3) and of 80–90 μm (2, 4) before (1, 2) and after (3, 4) the ultrasonic treatment respectively.

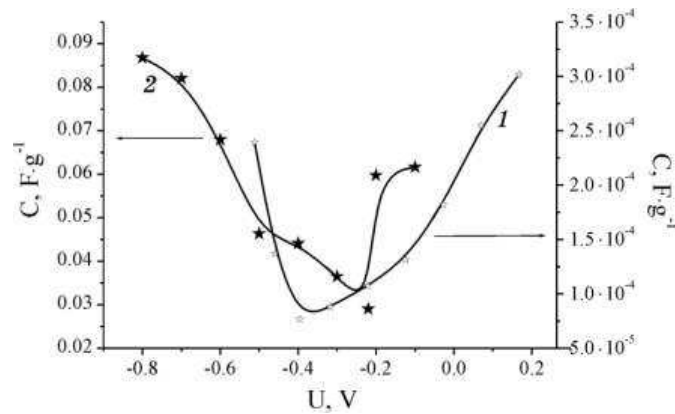


Fig. 8. Volt–farad dependence of SCR for FFC before (1) and after (2) the ultrasonic treatment.

adequately reflected in the $D(E_F)$ changes. The fact that dominant contribution to the value of R_{SC} brings the mobility of delocalized electrons, which depends on the type of fractal structure rather than on their concentration is the most probably a physical reason. This suggests that the time constant of $R_{SC}C_{SC}$ -link should be selected as the factor responsible for the measured value of C . It actually reflects the shunting of C_{SC} by the resistance of SCR. R_{SC} indicates the fact that an effective unblocking of the Helmholtz capacitance is observed, when the time of charge setting on ‘plates’ of C_{SC} is higher than the period of its oscillations.

TABLE 4. Fermi level position displacements after the ultrasonic treatment.

Nanoporous material	ΔF , eV
BCC (40–63 μm)	0.16
BCC (80–90 μm)	0.30
FCC (80–90 μm)	0.16

TABLE 5. Parameters of the first order Raman spectra for nanoporous BCC before and after the ultrasonic treatment.

Nanoporous material	μ_D , cm^{-1}	μ_G , cm^{-1}	I_D/I_G	$\delta\nu_D$, cm^{-1}	$\delta\nu_G$, cm^{-1}
BCC (40–63 μm) before UST	1303	1595	1.29	158	70
BCC (40–63 μm) after UST	1305	1592	1.27	145	73
BCC (80–90 μm) before UST	1307	1595	1.27	162	60
BCC (80–90 μm) after UST	1309	1597	1.36	148	53

Results of Raman shifts investigation are presented in Table 5 and in Fig. 9 and display in detail the physical nature of the observed changes caused by ultrasonic irradiation. One can see that in the first order spectra of the 40–63 μm size particles fraction, more than two-fold decrease of intensities (caused by ultrasonic irradiation) of D and G -bands is observed.

This indicates a possible carbon bonds disordering. In addition, the distance between the D - and G -bands reduces only for that dimension fractions.

However, the relative intensity of D -band (I_D/I_G) (which is an integral indicator of defects [27]) for the 40–63 μm fraction decreases after the ultrasonic influence unlike the 80–90 μm fraction, for which this option significantly increases. The opposite character of changes caused by UST for indicated fractions is typical for half-width of G -band ($\delta\nu_G$). This band is highly sensitive to structural disordering that caused by the distortion of angles and bond lengths [28]. Thus, the UST differently effects on defects, the distribution in different size fractions of carbon material and effects on its defective topology. The opposite character of changes for fractions with size of 40–63 μm and 80–90 μm after ultrasonic modification is observed in the second order Raman spectra. For the first fraction, intense wide band with a maximum at the frequency of 2481 cm^{-1} almost disappears, and for the second fraction, broadband appears at the frequency of 2607 cm^{-1} .

5. CONCLUSIONS

1. The action of ultrasound on carbon material particles leads to their

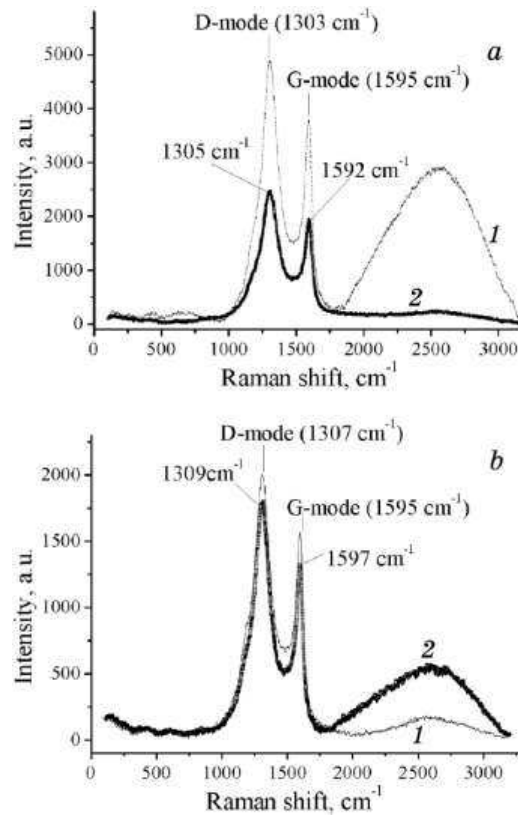


Fig. 9. Raman spectra taking for BCC fractions of 40–63 μm (a) and 80–90 μm (b) before (1) and after (2) the ultrasonic treatment.

crushing. Smaller size particles content increasing and content of other particles fractions decrease occurs as a result of this effect.

2. Proposed ultrasonic modification of nanoporous carbon is a convenient, cheap and effective way to improve specific capacity and power of supercapacitors based on it.

3. Significant improvement of operating characteristics is caused by an essential decrease of time constant of $R_{sc}C_{sc}$ -link of SCR in general and R_{sc} resistance in particular after ultrasonic treatment.

4. Changes of the EDL parameters are directly related to the change of fractal dimension, which, in turn, promotes increase of the percolation mobility of charge carriers with the given ultrasonic parameters.

REFERENCES

1. A. Kraytsberg and Y. Ein-Eli, *Adv. Energy Mater.*, **2**: 922 (2012).
2. B. Xu, D. Qian, Z. Wang, and Y. S. Meng, *Mater. Sci. Eng. R*, **73**, Nos. 5–6: 51

- (2012).
3. B. Ya. Venhryn, Z. A. Stotsko, I. I. Grygorchak, B. P. Bakhmatyuk, and S. I. Mudry, *Ultrason. Sonochem.*, **20**, No. 5: 1302 (2013).
 4. B. Ya. Venhryn, I. I. Grygorchak, Yu. O. Kulyk, and S. I. Mudry, *Mater. Sci.-Poland*, **31**, No. 1: 126 (2013).
 5. C.-C. Hu, W.-Y. Li, and J.-Y. Lin, *J. Power Sources*, **137**: 152 (2004).
 6. Feng-Chin Wu, Ru-Ling Tseng, Chi-Chang Hu, and Chen-Ching Wang, *J. Power Sources*, **144**: 302 (2005).
 7. K. Kierzek, E. Frackowiak, G. Lota, G. Gryglewicz, and J. Machnikowski, *Electrochim. Acta*, **49**: 515 (2004).
 8. S. L. Candelaria, R. Chen, Y.-H. Jeong, and G. Cao, *Energy Environ. Sci.*, **5**: 5619 (2012).
 9. P.-L. Taberna, G. Chevallier, P. Simon, D. Plée, and T. Aubert, *Mater. Res. Bull.*, **41**, No. 3: 478 (2006).
 10. C. Liang, Z. Li, and S. Dai, *Angew. Chem. Int. Ed.*, **47**: 3696 (2008).
 11. W. Xing, C. C. Huang, S. P. Zhuo, X. Yuan, G. Q. Wang, D. Hulicova-Jurcakova, Z. F. Yan, and G. Q. Lu, *Carbon*, **47**: 1715 (2009).
 12. M. Seredych, D. Hulicova-Jurcakova, G. Q. Lu, and T. J. Bandosz, *Carbon*, **46**: 1475 (2008).
 13. B. E. Conway, *Electrochemical Supercapacitors: Scientific Fundamentals and Technological Applications* (New York: Kluwer Academic-Plenum Publishing: 1999).
 14. S. Yoon, J. Lee, T. Hyeon, and S. M. Oh, *J. Electrochem. Soc.*, **147**: 2507 (2000).
 15. H. Gerischer, *J. Phys. Chem.*, **89**: 4249 (1985).
 16. S. Alexander, C. Laermans, R. Orbach, and H. M. Rosenberg, *Phys. Rev. B*, **28**, No. 8: 4615 (1983).
 17. A. I. Olemskoi and A. Ya. Flat, *Physics Uspekhi*, **36**, No. 12: 1087 (1993).
 18. É. A. Smorgonskaya, R. N. Kyutt, S. K. Gordeev, A. V. Grechinskaya, J. A. Kukushkin, and A. M. Danishevskii, *Phys. Solid State*, **42**: 1176 (2000).
 19. B. A. Agranat, M. N. Dubrovin, N. N. Khaevskii, H. I. Eskin, *Fundamentals of the Physics and Technology of Ultrasound* (Moscow: Vysshaya Shkola: 1987) (in Russian).
 20. I. V. Ostrovskii, A. B. Nadtochii, and A. A. Podolyan, *Semiconductors*, **36**, No. 4: 367 (2002).
 21. B. Hammouda, *J. Appl. Cryst.*, **43**, No. 4: 716 (2010).
 22. H. Schnablegger and Y. Singh, *The SAXS Guide. Getting Acquainted with the Principles* (Austria: Anton Paar: 2011).
 23. *Computational Photochemistry, Theoretical and Computational Chemistry* (Eds. M. Olivucci) (Amsterdam: Elsevier: 2005), vol. **16**, ch. III, p. 93.
 24. F. Collet, M. Bart, L. Serres, and J. Miriel, *Constr. Build. Mater.*, **22**, No. 6: 1271 (2008).
 25. Z. B. Stoynov, B. M. Grafov, B. S. Savova-Stoynova, and V. V. Elkin, *Electrochemical Impedance* (Moscow: Nauka: 1991) (in Russian).
 26. H. Gerischer, R. McIntyre, D. Scherson, and W. Storck, *J. Phys. Chem.*, **91**, No. 7: 1930 (1987).
 27. É. A. Smorgonskaya, T. K. Zvonareva, E. I. Ivanova, I. I. Novak, and V. I. Ivanov-Omskii, *Phys. Solid State*, **45**, No. 9: 1658 (2003).
 28. C. Casiraghi, A. C. Ferrari, and J. Robertson, *Phys. Rev. B*, **72**, No. 8: 085401 (2005).